euronoise

Acoustic and aerodynamic dissipations induced by a sound wave-impacted Helmholtz resonator

Jean-Michel Roche, Laurent Leylekian and François Vuillot

ONERA, BP 72 - 29 avenue de la Division Leclerc, 92322 Châtillon, France
jean-michel.roche@onera.fr

Nowadays, the use of resonant acoustic liners is one of the most efficient ways to reduce aircraft engine noise, especially fan noise which can reach more than 140 dB. The purpose of the work introduced herein is to revisit the normal incidence acoustic absorption of these liners: 2D planar direct numerical simulations (DNS) are performed with the CEDRE code, a Navier-Stokes equations solver developed by Onera, to evaluate the acoustic dissipation of a Helmholtz resonator. The response of the resonator is computed for several incident sound pressure levels from 80 to 150 dB. It is checked that for the lowest SPLs, the acoustic absorption is based on viscous wall friction and radiation through the resonator opening: these mechanisms are linear. For the highest SPLs however, a substantial part of the absorption is provided by nonlinear effects, generated by the shedding of micro-vortices at the opening mouths which converts the acoustic energy in kinetic rotational energy, eventually dissipated into heat by molecular viscosity. For every simulated case, the efficiency of the dissipation is quantified by the calculation of the absorption coefficient. The weight of the nonlinear mechanisms on the global absorption is discussed, especially for the "intermediate" SPLs.

1 Introduction

Several techniques are commonly used today to reduce aircraft engine noise: direct action on the source, improvement of the directivity, acoustic absorption by porous or resonant liners. In this latter case, liners, such as perforated honeycomb liners, are put in the inlet nacelle to reduce the fan noise, a tone noise which can reach more than 140 dB and which is critical for the take-off and landing phases because of its directivity.

In order to improve the acoustic treatment efficiency, it is crucial to get a full understanding of its absorption mechanisms. Most of current prediction models rely on empirical or semi-empirical concepts, and are not totally reliable. Acoustic performances of liners are indeed greatly affected by nonlinear effects, as much due to high sound pressure levels (SPL) as to the interactions between sound and grazing air flows. The purpose of the work introduced herein is to evaluate the first one of these two nonlinear effects, by simulating the response of a Helmholtz resonator to harmonic acoustic waves at several SPLs.

2 Properties of the 2D resonator

2.1 Computation domain

Our computation domain, as shown in Fig.1., is a normal incidence impedance tube.

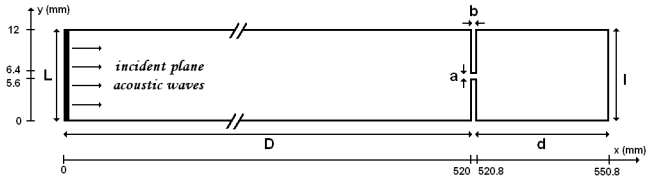

Fig.1. The computation domain.

Acoustic waves are propagated in a 520 mm × 12 mm tube, and impact the resonator. The tube length is chosen so that the resonator is more than one wavelength away from the inlet boundary at the lowest excitation acoustic frequency (which will be specified in 2.2). Its height cuts off the higher order modes at the chosen frequencies, thus allows only plane waves propagation.

The openings of perforated honeycomb liners are usually very small. Therefore, even if it might lead to numerical issues, such as long computational times, the size of the resonator studied herein is the one of a typical industrial liner: a = b = 0.8 mm; d = 30 mm; l = 12 mm.

2.2 Theoretical resonance frequency

Given the dimensions of the hole, it is classically assumed that the air flow is incompressible in the resonator opening; moreover, the continuity of pressures and the conservation of volume fluxes at the opening / cavity interface are assumed. Under these assumptions, the resonator reactance is given by the simplified line impedance theory [1]:

$$X_{res} = \rho \cdot c \cdot \left(k \cdot (b + \Delta b) - \frac{a}{l} \cdot \frac{1}{\tan(kd)} \right) \qquad (1)$$

b, a, l and d are defined in Fig.1., ρ is the density of air, c the speed of sound, k the acoustic wave number, and Δb the end correction at the resonator mouth. The adaptation of Rayleigh's [2] three-dimensional theory to a 2D geometry gives:

$$\Delta b = \left(\frac{\pi}{4} \right)^{1/3} a \qquad (2)$$

Fig.2. shows that the annulment of the resonator reactance happens at 1.7 kHz. This frequency is the Helmholtz resonance frequency (f_H).

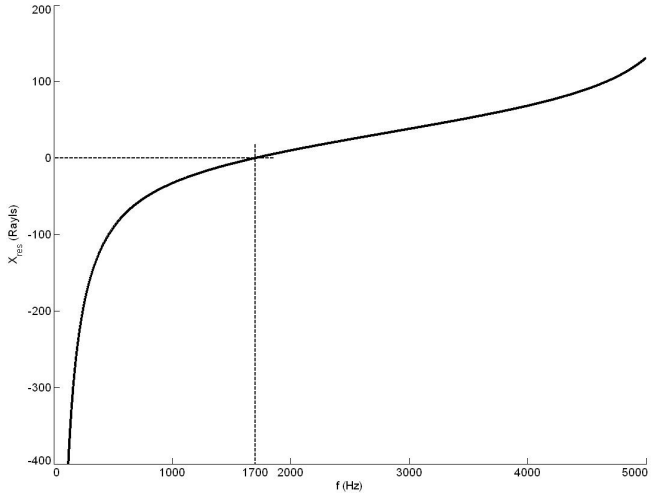

Fig.2. Time variation of the resonator reactance.

Maximum absorption is expected for f_H. In this paper, three acoustic frequencies are chosen: the Helmholtz frequency (1.7 kHz), the quarter-wave frequency, exclusively

depending on the depth of the resonator (f_λ = 2.83 kHz), and an arbitrarily chosen frequency (f_0 = 1.0 kHz).

3 Computational model

3.1 Grid design

The direct numerical simulations are carried out with the Onera CEDRE code. The governing equations are the compressible Navier-Stokes and energy equations:

$$\frac{\partial \rho}{\partial t} + \frac{\partial}{\partial x_j}\left(\rho u_j\right) = 0 \tag{3}$$

$$\frac{\partial}{\partial t}\left(\rho u_i\right) + \frac{\partial}{\partial x_j}\left(\rho u_i u_j\right) + \frac{\partial p}{\partial x_i} - \frac{\partial \tau_{ij}}{\partial x_j} = 0 \tag{4}$$

$$\frac{\partial p}{\partial t} + u_j \frac{\partial p}{\partial x_j} + \rho c^2 \frac{\partial u_j}{\partial x_j} = 0 \tag{5}$$

$$\tau_{ij} = \mu\left(\frac{\partial u_i}{\partial x_j} + \frac{\partial u_j}{\partial x_i}\right) - \frac{2}{3}\mu \frac{\partial u_i}{\partial x_i} \tag{6}$$

Initially, the fluid is at rest, and characterized by the following physical properties: P = 101,198 Pa; T = 288 K. The acoustic excitation in the duct inlet is modelled by sinusoidal varying mass and energy fluxes, assigned to the first row of rectangular mesh elements. The inlet wall is non-reflective; the other walls are set adiabatic.

The choice of an explicit Runge-Kutta 2 time integration scheme considerably reduces numerical dissipation. However, the mesh must be refined enough to enable the propagation of acoustic waves. The tube is meshed with triangles of height 0.8 mm, at the rate of respectively 250, 150 and 425 mesh nodes by wavelengths for f_H, f_λ and f_0. Around the resonator opening, an even more refined grid is required, since the dissipation mechanisms have to be properly simulated and observed. Fig.3. shows the six mesh areas of the grid inside the resonator.

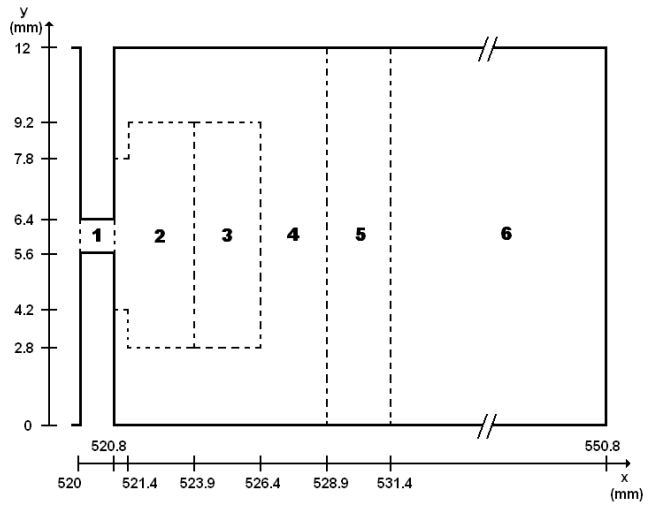

Fig.3. Mesh grid inside the resonator.

Particular attention is paid to the flowfield in the opening. As long as it remains linear, the oscillatory air flow through the slit is expected to be linear, and characterized by a Stokes viscous boundary layer, the thickness of which is given by [3]:

$$\delta = \sqrt{\frac{\nu}{\pi f}} \tag{7}$$

where ν is the air kinematic viscosity. In order to get a fine resolution, the opening walls are meshed with 0.008 mm side squares: it represents 5 mesh nodes by layer thickness for the most critical case, that is to say for f_λ (δ = 0.040 mm). Outside of the viscous layer, area 1 is meshed with triangles of height 0.008 mm. Consequently, the opening grid includes 10,000 mesh elements over all. The five other areas are less refined: $\Delta x_{area\ 2}$ = 0.02 mm; $\Delta x_{area\ 3}$ = 0.04 mm; $\Delta x_{area\ 4}$ = 0.10 mm; $\Delta x_{area\ 5}$ = 0.40 mm; $\Delta x_{area\ 6}$ = 0.80 mm. Between x = 490 mm and x = 520 mm, on the left of the resonator mouth, the grid is exactly the same, so that the global computation domain is meshed with about 200,000 mesh cells.

3.2 Choice of the computation time step

The time step is constant for the whole geometry. It is fixed by the smallest size mesh, as the stability CFL (Courant-Friedrich-Lewy) condition requires. The CEDRE code explicit RK 2 time integration scheme needs a CFL inferior to 0.5. Thus, the chosen step time is $\Delta t = 10^{-8}$ s.

4 Study of the effect of SPL on acoustic dissipation

Eighteen direct numerical simulations are performed, at the three chosen frequencies, and for six sound pressure levels: 80, 110, 120, 130, 140 and 150 dB. This large panel of SPLs should enable us to identify the different dissipation mechanisms of the resonator, and to highlight the transition between linear and nonlinear effects. For every studied case, the absorption coefficient is calculated, in order to quantify the efficiency of the acoustic dissipation. Particular attention is paid to the weight of nonlinear mechanisms on the global absorption.

4.1 Acoustic dissipation at "low SPL"

For the 80 dB sound pressure level, it is checked that the air flow is laminar and that it oscillates in the opening at the incident acoustic frequency. The longitudinal velocity profile in the opening (along x = 520.4 mm) at the beginning of a cycle and at the end of the first quarter of it, is provided in Fig.4. The same profile is observed for every frequency, the thickness of the boundary layer and the values of velocity varying with f.

A Stokes viscous layer appears along the walls. Based on the profile provided in Fig.4., its thickness is in good agreement with the analytic model (δ ≈ 0.050 mm). Obviously, the values of longitudinal velocity are really low. Over a quarter of period, the x-velocity in the center of the slit varies between 0.004 m/s and 0.018 m/s. In the layer, maximal values do not exceed 0.020 m/s.

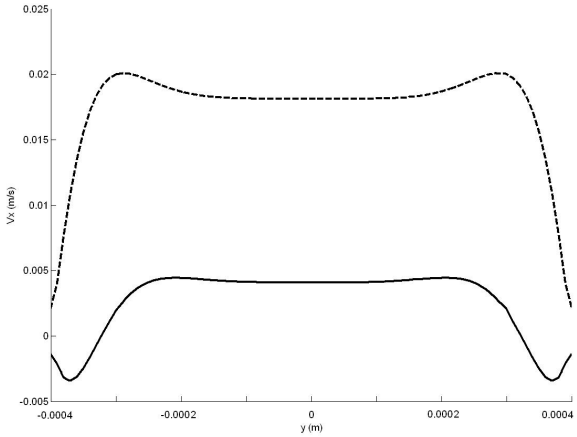

Fig.4. Instantaneous x-velocity in the opening (x = 520.4 mm). SPL = 80 dB; f = 1.7 kHz. Solid line: $t = t_0$; dashed line: $t = t_0 + 1/(4.f)$

These characteristics of the flowfield are confirmed by Fig.5. and Fig.6 which respectively provide the norm of the instantaneous velocity vector and streamline pattern around the opening.

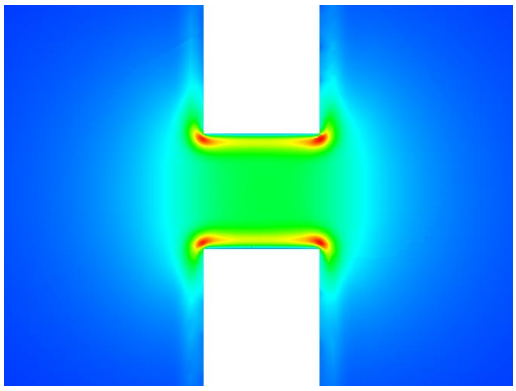

Fig.5. Norm of instantaneous velocity vector around the opening. SPL = 80 dB; f = 1.7 kHz

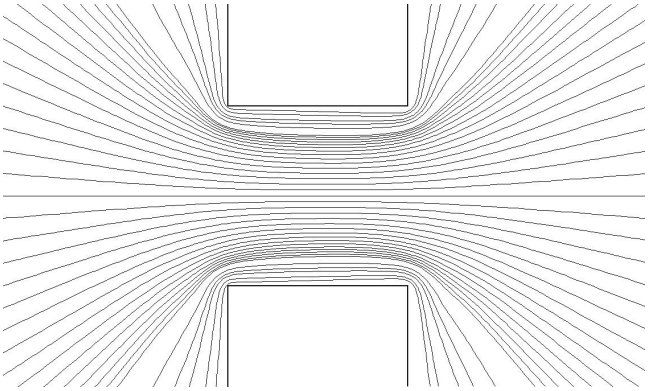

Fig.6. Instantaneous streamline pattern around the opening. SPL = 80 dB; f = 1.7 kHz.

The profiles of the instantaneous velocity and streamline pattern through the resonator opening are characteristics of the classic dissipation mechanisms of viscous wall friction and acoustic radiation.

4.2 Acoustic dissipation at "high SPL"

For both 140 and 150 dB sound pressure levels, the air flow is not laminar anymore. As Tam describes it in previous studies [4, 5, 6], and as it can be seen in Fig.7. and Fig.8., micro vortices are shed on each side of the resonator mouth: these vortices are either attached vortices, internally generated along the opening walls, or free vortices, externally generated at the opening corners. Free vortices then merge in counter-rotating pairs and move away from the resonator.

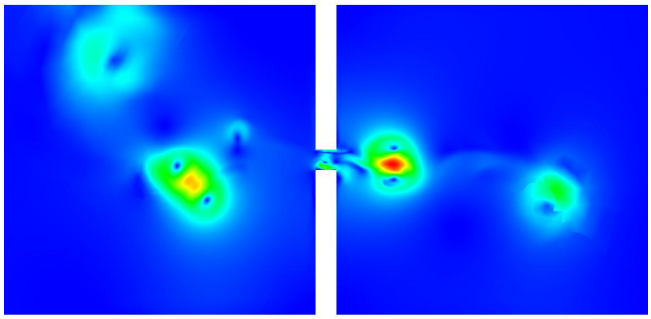

Fig.7. Norm of instantaneous velocity vector. SPL = 150 dB; f = 1.7 kHz

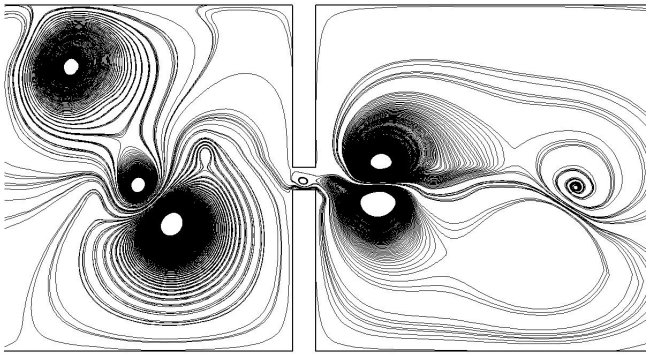

Fig.8. Instantaneous streamline pattern. SPL = 150 dB; f = 1.7 kHz

The shedding of vortices globally remains periodic, and it is found that the shedding frequency is the very incident acoustic frequency. However, the instantaneous velocity profile is ultimately quite unpredictable.

The instantaneous flow velocity is much higher, almost reaching a 0.15 Mach number in the opening. The maximal rotational velocity of the micro vortices is high too (about 0.05 Mach number).

A new dissipation mechanism is pointed out: the conversion of the acoustic energy in kinetic rotational energy, eventually dissipated into heat by molecular viscosity.

4.3 Acoustic dissipation mechanism at "intermediate SPLs"

The 110, 120 and 130 dB sound pressure levels may be regarded as "intermediate" SPL. It is found that no vortices are generated at 110 and 120 dB. Though acoustic velocities are quite higher, the air flow remains laminar and the streamline pattern is exactly the same than the 80 dB one.

Micro vortices only appear at 130 dB. However, as shown in Fig.9. and Fig.10., they are not shed away from the opening: on the contrary, they remain confined at the resonator corners. The velocities are much weaker than those observed at 140 and 150 dB (no more than 5 m/s).

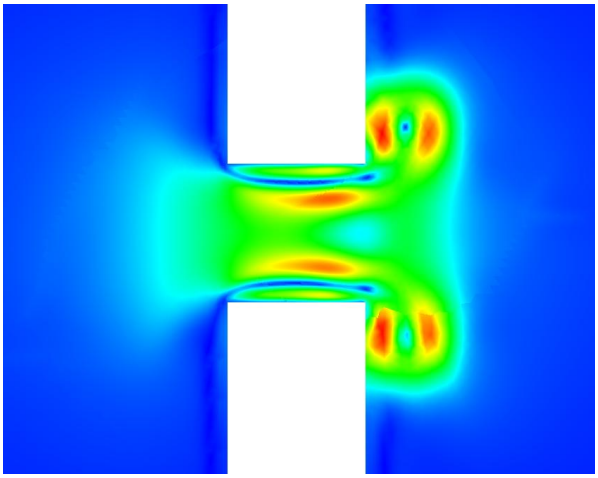

Fig.9. Norm of instantaneous velocity vector around the opening. SPL = 130 dB; f = 1.7 kHz

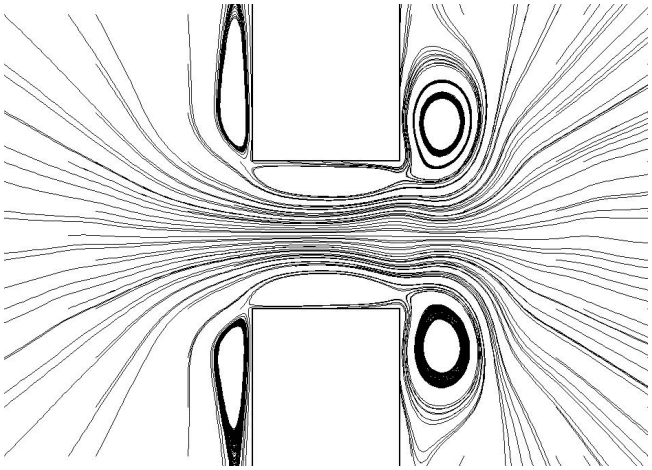

Fig.10. Instantaneous streamline pattern around the opening. SPL = 130 dB; f = 1.7 kHz

4.4 Absorption coefficient calculation

Depending on the sound pressure level, the absorption coefficient of the Helmholtz resonator is to be calculated differently. Numerical sensors are placed in the duct, so that the linearity of the time pressure signals is checked. As long as they remain linear, the absorption can be quantified with the two-microphone transfer function technique (i.e. the normal incidence Kundt tube method). For several pairs of sensors, the time pressure signals are fitted by sine curves with the linear least squares fitting technique; once the "$p_{imax}\times\sin(\omega t+\varphi_i)$" look-alike equations are found, the phase difference $\Delta\varphi$ and the ratio between the maximal amplitudes are calculated. It then leads to the transfer function h_{ij} (Eq.(8)), and ultimately to the reflection and absorption coefficients r and α (Eq.(9)).

$$h_{ij} = \left|\frac{p_{j\max}}{p_{i\max}}\right| \cdot e^{i\Delta\varphi} \tag{8}$$

$$\alpha = 1 - |r|^2 = 1 - \left| e^{2ikx_i} \frac{e^{-iks} - h_{ij}}{h_{ij} - e^{iks}} \right|^2 \tag{9}$$

x_i is the distance between the resonator and the most distant sensor, and s the distance between the two sensors.

As expected, the 80 dB time signals are linear: they are perfectly fitted by sine curves, with the linear least squares fitting technique. The 110 and 120 dB signals happen to be exact multiples of the 80 dB ones, which sets their linearity. Thus, the two-microphone transfer function method is valid for these three SPLs. Theoretically, given that the ratio between the maximal amplitudes of the two sensors and the phase difference remain constant for these SPLs, the absorption coefficient is expected to remain constant.

As it was also expected, the highest studied SPLs (140 and 150 dB) time pressure signals are definitely nonlinear so that the two-microphone transfer technique is now irrelevant. The effects of nonlinearity, as shown in Fig.11., are a non constant amplitude, an alteration of the sinusoidal shape, and a substantial phase difference with the theoretical linear time signal.

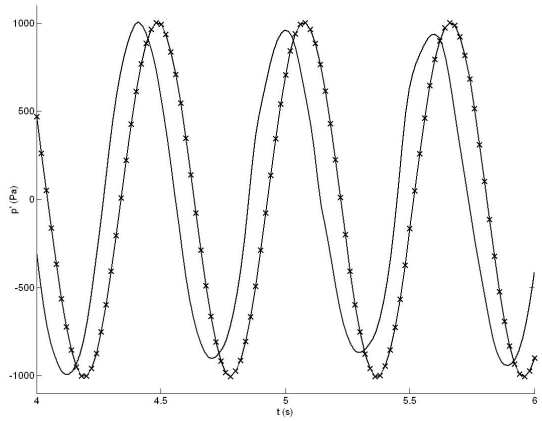

Fig.11. Instantaneous pressure. Solid line: SPL = 150 dB; f = 1.7 kHz; line with crosses: theoretical linear time signal for the same SPL and frequency

For these high SPLs, the approach chosen in this paper is to split the global dissipated energy into a linear contribution E_{linear} and a nonlinear one $E_{nonlinear}$, due to vortex shedding. The very principle of linearity of the first contribution enables the calculation of E_{linear} from the incident energy (Eq.(10)) and the absorption coefficients found at 80 dB (Eq.(11)).

$$E_{incident} = \frac{\overline{p'^2}}{\rho_0 c_0} L \tag{10}$$

$$E_{linear} = \alpha_{80dB} \times E_{incident} \tag{11}$$

For the second contribution, $E_{nonlinear}$, the average kinetic energy K associated with a shed micro vortex, defined by its radius R and its rotational velocity v_θ, is to be calculated (Eq.(12)), following Tam's method [4, 5, 6].

$$K = <\pi \int_0^R \rho(r) \cdot v_\theta^{\,2}(r) r dr> \tag{12}$$

The nonlinear energy is then given by Eq.(13):

$$E_{nonlinear} = E_{vortex} = \frac{N \cdot K}{T} \tag{13}$$

with N the number of vortices per shedding period T (which actually is the acoustic waves period).

The ratio between the sum of both dissipation energies and the incident energy eventually leads to the absorption coefficient (Eq.(14)).

$$\alpha_{150dB} = \frac{E_{linear} + E_{nonlinear}}{E_{incident}} = \alpha_{80dB} + \frac{E_{vortex}}{E_{incident}} \tag{14}$$

The nonlinearity of the 130 dB time pressure signals is not as obvious as it is for the 140 and 150 dB cases. However, as observed in the previous paragraph, the 130 dB dissipation also relies on the vortex shedding mechanism. Therefore, the absorption coefficient is calculated with the linear / nonlinear splitting.

4.5 Efficiency of the dissipation

Table 1 and Table 2 provide the results of the eighteen direct numerical simulations. The absorption coefficients are calculated as explained in 4.4.

	80 dB	110 dB	120 dB
1.0 kHz	0.12	0.12	0.12
1.7 kHz	0.26	0.26	0.26
2.83 kHz	0.11	0.10	0.11

Table 1 Absorption coefficients at "low" SPLs

For a given frequency, α does not vary with the SPL. The values are quite weak: the linear dissipation mechanism is not very efficient. No more than one quarter of the incident acoustic energy is dissipated.

	130 dB	140 dB	150 dB
1.0 kHz	$\alpha_{nonlin} = 0.08$ $\alpha_{global} = 0.20$	$\alpha_{nonlin} = 0.13$ $\alpha_{global} = 0.25$	$\alpha_{nonlin} = 0.19$ $\alpha_{global} = 0.31$
1.7 Hz	$\alpha_{nonlin} = 0.18$ $\alpha_{global} = 0.44$	$\alpha_{nonlin} = 0.32$ $\alpha_{global} = 0.58$	$\alpha_{nonlin} = 0.44$ $\alpha_{global} = 0.70$
2.83 kHz	$\alpha_{nonlin} = 0.06$ $\alpha_{global} = 0.17$	$\alpha_{nonlin} = 0.11$ $\alpha_{global} = 0.22$	$\alpha_{nonlin} = 0.17$ $\alpha_{global} = 0.28$

Table 2 Nonlinear and global absorption coefficients at "high" SPLs

It is checked that the absorption coefficient of the Helmholtz resonator significantly increases when vortices are shed, as shown in Fig.12. which provides the variation of the absorption coefficient with the sound pressure level, for every frequency. For the 150 dB SPL, at the Helmholtz frequency, which gives the best absorption frequency, 70 per cent of the incident acoustic energy is dissipated. The absorption is three times more efficient than it is for a low SPL.

It is also noticed that the ratio between the nonlinear contribution and the global absorption increases with the sound pressure level. The part of incident energy dissipated through the opening walls by viscous friction and acoustic radiation is then quite weak, but still remains significant.

The results quantifying the efficiency of the vortex shedding dissipation mechanism in comparison with the linear dissipation mechanisms are in good agreement with Tam's two-dimensional results. However, the value of the maximal absorption coefficient (0.70 for SPL = 150 dB and $f = f_H$) seems to suggest that the Helmholtz frequency might not be the exact "absolute" maximal absorption frequency. On the other hand, it is definitely not the quarter-wave frequency either. More direct numerical simulations, for other acoustic frequencies, are obviously required.

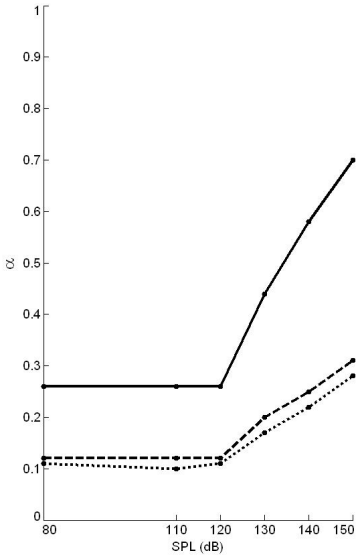

Fig.12. Variation of absorption coefficients with sound pressure levels. Solid line: f = 1.7 kHz; dashed line: f = 1.0 kHz; dotted line: f = 2.83 kHz.

5 Conclusion

The nonlinear dissipation mechanism of vortex shedding is obviously crucial in the global acoustic absorption of resonant liners such as Helmholtz resonators. Further studies will follow in order to bring better understanding of these non linearities. We then intend to compare the present results with three-dimensional ones. Eventually, the second kind of nonlinear effects, that is to say the interaction between sound and grazing air flow, will be studied.

Acknowledgments

The authors thank Dr. Yves Aurégan of the Laboratoire d'Acoustique de l'Université du Maine, for his comments and suggestions on this work.

References

[1] B. Haÿne Lecocq, "Contribution à l'étude du comportement acoustique de matériaux présentant des cavités débouchantes", *thèse ENSAM* (2006)

[2] Rayleigh, "On the theory of resonators", *Philosophical transactions of the Royal Society* (1870)

[3] NATO Research and Technology Organization, "Annex C – The Acoustic boundary layer" (2006)

[4] Tam C.K.W., Kurbatskii K.A., "Microfluid dynamics and acoustics of resonant liners", *AIAA Journal, Vol.38, No.8, 1331-1339* (2000)

[5] Tam C.K.W., Kurbatskii K.A., Ahuja K.K., Gaeta R.J., "A numerical and experimental investigation of the dissipation mechanisms of resonant acoustic liners", *JSV 245(3), 545-557* (2001)

[6] Tam C.K.W., Ju H., Jones M.G., Watson W.R., Parott T.L., "A computational and experimental study of slit resonators", *JSV 284, 947-984* (2005)